International Journal of Microwave and Wireless Technologies

cambridge.org/mrf

An integrated polarization-reconfigurable pulse transmitter based on a reconfigurable pulse-triggered network

Manman Cui[1], Jun-Hao Lai[2,3] and Huai-Tian Zhou[2,3]

[1]School of Medical Information Engineering and the Intelligent Chinese Medicine Research Institute, Guangzhou University of Chinese Medicine, Guangzhou, China; [2]School of Integrated Circuits, Guangdong University of Technology, Guangzhou, China and [3]State Key Laboratory of Millimeter Waves, Nanjing, China

Research Paper

Cite this article: Cui M, Lai J-H, Zhou H-T (2025) An integrated polarization-reconfigurable pulse transmitter based on a reconfigurable pulse-triggered network. *International Journal of Microwave and Wireless Technologies* **17**(8), 1291–1297. https://doi.org/10.1017/S175907872510278X

Received: 18 June 2025
Revised: 8 December 2025
Accepted: 10 December 2025

Keywords:
active integrated antenna; polarization reconfigurability; pulse transmitter; self-oscillation

Corresponding author: Manman Cui; Email: cmm@gzucm.edu.cn

Abstract

This work proposes an integrated pulse transmitter with polarization reconfigurability. A reconfigurable pulse-triggered network is designed and seamlessly integrated with a dual-polarized radiator within the compact transmitter structure. This integration allows the radiator to sequentially perform DC charge accumulation, pulse oscillation, and radiation during each pulse cycle. Moreover, the reconfigurable pulse-triggered network introduces two operating modes, enabling the pulse transmitter to switch between different polarization states. Experiments demonstrate that the proposed pulse transmitter can directly convert DC energy into radiated pulses with switchable polarization modes. The pulse signal with a peak-to-peak voltage of 1.6 V is received in the −45° polarization direction at 1.5 m under mode 1, and switches to +45° polarization with a peak-to-peak voltage of 1.6 V under mode 2.

Introduction

Conventional wireless transmitters necessitate separate oscillator-antenna configurations. Recent advances in co-design methodologies integrate these functional blocks into unified topologies, termed self-oscillating active integrated antennas (AIAs), delivering significant benefits in miniaturization, high integration, and manufacturing economy. Such integrated solutions have demonstrated critical utility across wireless power transfer (WPT) [1, 2], radio frequency identification [3–5], etc.

Many techniques have been implemented to enhance the oscillation and radiation performance of self-oscillating AIAs, including cross-coupled pair [6, 7], electrically small conical folded dipole antenna [8], backward-radiating helical antenna [9], substrate integrated waveguide (SIW) [10], composite right-/left-handed (CRLH) resonator [11], circuit multiplexing [12], and coherent stimulated emission [13, 14]. The cross-coupled pair of transistors embedded with *LC* resonators can achieve harmonic suppression in the self-oscillating AIA, which reduces the DC power consumption [7]. The SIW technique is employed in [10] to design a self-diplexing antenna in the self-oscillating AIA, which realizes concurrent dual-frequency signal generation and radiation. In [11], a high-quality (Q) factor CRLH resonator is used to excite the radiator to boost its effective isotropic radiated power. In [12], a self-oscillating circuit is embedded and multiplexed in a dual-loop radiator to achieve dual-band operation. In [14], an extensible self-oscillating AIA array is designed based on coherent stimulated emission theory, which is able to boost the power level of the output pulse.

Reconfigurable techniques have been implemented in self-oscillating AIA designs to enhance controllability [15–20]. In [16], diodes are used to change the resonant frequency of the radiators, enabling the self-oscillating AIA to achieve frequency reconfigurability. In [18], several PIN diodes are inserted between two patch antennas and several delay lines, which control the phase of the current on the two antennas to obtain three radiation beams. PIN diodes are also embedded at four corners of the radiating element to control the shape of the patch antenna, which enables polarization reconfigurability of the feedback loop oscillator-type AIA in [20]. However, these self-oscillating AIAs are fundamentally limited to continuous wave (CW) generation with restricted operating power.

In contrast to the existing polarization reconfiguration methods for CW self-oscillating AIA, this work introduces a novel polarization reconfiguration approach applicable to pulsed self-oscillating AIA based on a pulse-triggered network. The proposed design integrates a reconfigurable pulse-triggered network with a dual-polarized radiator. This integration not only facilitates the direct conversion of direct current (DC) energy into radiated pulses within a highly integrated system but also enables polarization reconfigurability. The dual-polarized radiator serves dual roles as both the DC energy storage element and the radiator for the pulse-triggered network, supporting pulse oscillation and radiation with the desired polarization characteristics.

© The Author(s), 2025. Published by Cambridge University Press in association with The European Microwave Association.

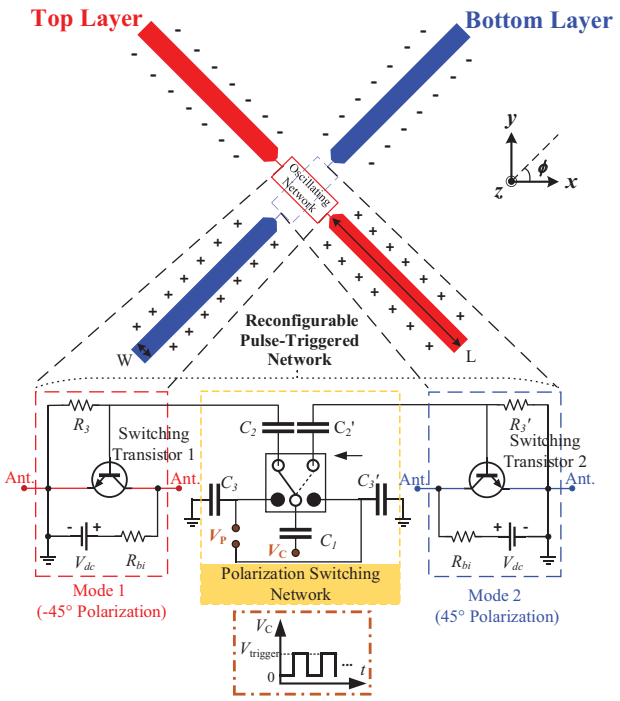


Figure 1. Schematic diagram of the proposed integrated polarization-reconfigurable pulse transmitter.

Design of the pulse transmitter

The proposed polarization-reconfigurable pulse transmitter integrates a dual-polarized dipole radiator with a reconfigurable pulse-triggered network, as illustrated in Fig. 1. The pulse transmitter is a periodic pulse source in which each working cycle consists of a charging phase and an oscillating phase. The reconfigurable pulse-triggered network aims to charge the dipole radiator during the charging phase and stimulate pulse oscillation and radiation during the oscillating phase. Specifically, when the switching transistor (Switching transistor 1 or Switching transistor 2) is off, which isolates the two arms of the dipole radiator, electric charges can be accumulated in the dipole radiator working as a capacitor (charging phase). The switching transistors are controlled by a low-frequency control signal V_C through a polarization-switching network. When V_C changes to a high-level voltage that activates the switching transistor to be on, the dipole radiator would be short-circuited, and the current oscillates on the radiator, and pulse radiation occurs (oscillating phase). Moreover, the polarization switching network is controlled by another bias voltage V_p in order to selectively trigger the switching transistor 1 (mode 1, dipole radiator on the top layer with −45° polarization) or switching transistor 2 (mode 2, dipole radiator on the bottom layer with 45° polarization) for pulse oscillation and radiation in the desired polarization direction, thus enabling polarization reconfigurability. In order to improve the isolation between the two polarizations, both arms of the dipole radiators are sharpened to remove the overlapping areas between the two dipole radiators, thereby reducing the coupling effect.

The working process of the proposed pulse transmitter is detailed as follows. Each switching transistor is embedded between the two arms of a dipole radiator. It is first in the off state to enable the pulse transmitter to work in the charging phase, as depicted in Fig. 2(a). In this case, the dipole radiators would be first charged by the DC power supply V_{DC} through the bias resistors R_{bi} in order to store the energy within the capacitive region of the radiators. Then, the polarization switching network will introduce a control signal V_c to one of the switching transistors to switch the pulse transmitter from the charging phase to the oscillating phase. Specifically, once the voltage of the control signal reaches the threshold voltage $V_{trigger}$, the target switching transistor would be activated, and the two arms of the corresponding dipole radiator would be suddenly connected. As a result, an oscillating current would be generated on the radiator, and a pulse would be radiated. In this way, the stored DC energy could be converted into a radiation pulse with a specific polarization. When the voltage of the control signal drops back to 0, the switching transistor becomes off, and the dipole radiator would be charged again, entering the next charging-oscillating cycle. The pulse repetition period is consistent with the operating cycle of the switching transistor, which is determined by the control signal V_C. Moreover, the frequency of the oscillation and radiation of the pulse is determined by the resonant frequency of the dipole radiator, as well as the intrinsic capacitance and parasitic elements of the switching transistor.

The polarization switching network in the reconfigurable pulse-triggered network is expected to enable the transition between two operating modes of the proposed design, thereby achieving polarization reconfigurability. It is designed to activate the target switching transistor and excite the pulse transmitter to generate radiation pulses with the desired polarization. In the switching network shown in Fig. 1(a), a SPDT switch is used, which is connected to the two switching transistors through the capacitors C_2 and C_2', respectively. It introduces the control signal V_C from its RFC port and transmits the control signal to activate the target switching transistor. The SPDT switch is controlled by the bias voltage V_P. When the bias voltage V_P is set to a high voltage level, the pulse transmitter would work in mode 1, where the electric charges oscillate in the dipole radiator on the top layer, generating an oscillating current that radiates a pulse with −45° polarization, as shown in Fig. 2(a). When V_C turns to a low voltage level, the pulse transmitter would transition to mode 2, where the oscillating current would be generated in the dipole radiator on the bottom layer, resulting in the emission of a pulse with 45° polarization, as shown in Fig. 2(b). In this way, the proposed pulse transmitter achieves polarization reconfigurability.

The polarization-reconfigurable pulse transmitter is designed on the FR4 substrate with a thickness of 1.2 mm, dielectric constants of 4.4, and a loss tangent of 0.02. In this example, the dual-polarized radiator is designed to work at 500 MHz. The length of each arm of the dipole radiator is determined by the resonant frequency of the passive dipole radiator, which is 126 mm. The width of each arm is optimized to ensure a sufficiently large equivalent capacitance of the antenna, consequently ensuring a large DC energy storage capacity for high output pulse voltage in the co-polar direction, while avoiding an increase in the cross-polar radiation. The width of each arm in this design example is set to be 8.5 mm. In order to obtain the performance of the radiator, the excitation ports are used to replace the pulse-triggered network, which is set between the two arms of the dipole radiators. The simulated *S*-parameters of the passive dual-polarized radiator are shown in Fig. 3, and the radiation patterns with realized gain are shown in Fig. 4. As seen, good isolation and orthogonal polarization are achieved. In addition, the surface current distributions of the radiator at the two operating modes are depicted in Fig. 5. Subsequently,

https://doi.org/10.1017/S175907872510278X Published online by Cambridge University Press

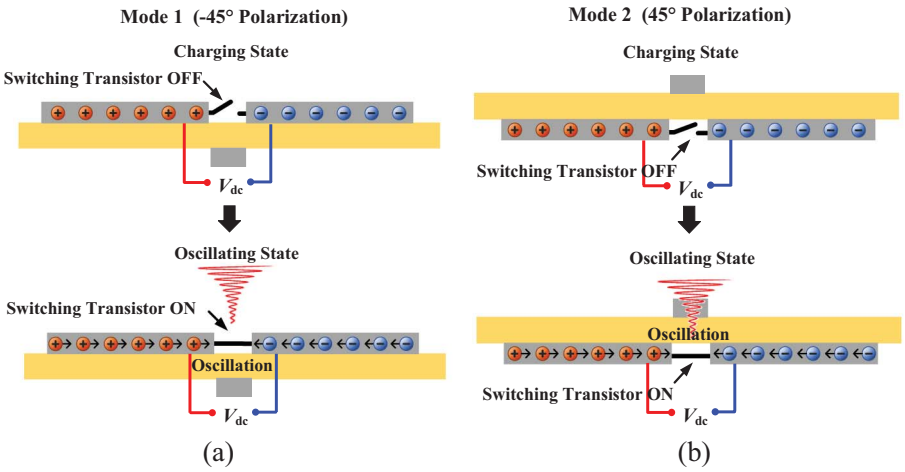


Figure 2. Working principle of the proposed pulse transmitter operating in (a) mode 1 and (b) mode 2.

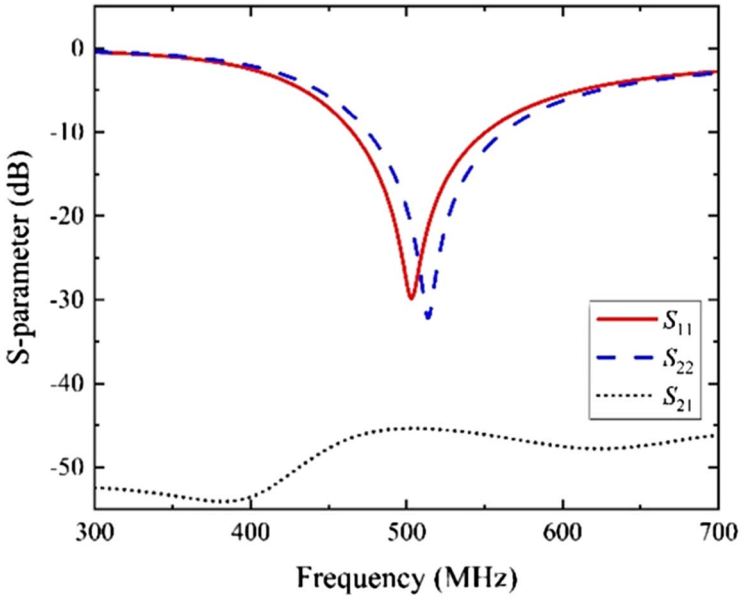


Figure 3. *S*-parameter of the passive dual-polarized radiator.

in order to further simulate the pulse transmitter, ideal voltage-controlled switches are utilized in the simulation, which combines the full-wave simulator and circuit simulator. A control signal V_C with a period of 100 ns and a duty cycle of 50% is used. Fig. 6(a) shows the simulated results of the proposed pulse transmitter working in mode 1 when V_P is set to a high voltage level. As seen, the dipole radiator on the top layer is first charged, as indicated by $V_{\text{Dipole-Top layer}}$ (e.g., 52–102 ns), and then is short-circuited for pulse oscillation and radiation (e.g., 102–152 ns) during each working cycle. The pulse repetition period of the proposed design is 100 ns, which is the same as the control signal V_C. Moreover, the pulse with −45° polarization is radiated with negligible cross polarization (45°). When V_P is set to a low voltage level, the proposed pulse transmitter is reconfigured to work in mode 2, as shown in Fig. 6(b). Oscillation and radiation occur in the dipole radiator on the bottom layer, and the pulse with 45° polarization is radiated with negligible cross polarization (−45°). In addition, the efficiency of the pulse transmitter is calculated to be about 37% according to the periodic transient signal.

Implementation and experiment

To implement the proposed design, the avalanche transistor FMMT413 is adopted as the switching transistor in the reconfigurable pulse-triggered network, so as to switch the operating state of the pulse transmitter between the charging phase and the oscillating phase. The fabricated pulse transmitter and the details of the reconfigurable pulse-triggered network are presented in Fig. 7. In the experiment, the DC power supply V_{DC} of 165 V is applied to charge the dipole radiators and bias the transistor FMMT413 to the critical avalanche state. It should be noted that the bias voltage across the avalanche transistor should be a little bit lower than the breakdown voltage of the transistor to ensure the critical breakdown state. Under this condition, the avalanche transistor can be triggered by the control signal to break down and short-circuit the two arms of the dipole radiator, thereby generating oscillation and radiation. The resistors R_1 and R_1' with large resistance are deployed in parallel at the base of the transistors to avoid current passing through the base. Besides, in the polarization switching network, the GaAs switch HMC544, with the advantage of low

https://doi.org/10.1017/S175907872510278X Published online by Cambridge University Press

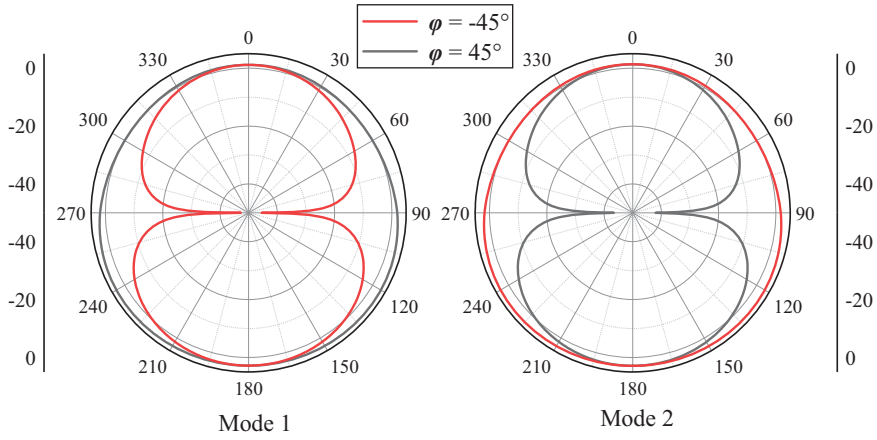


Figure 4. Radiation patterns with the realized gain of the dual-polarized radiator when the pulse transmitter works in mode 1 and mode 2.

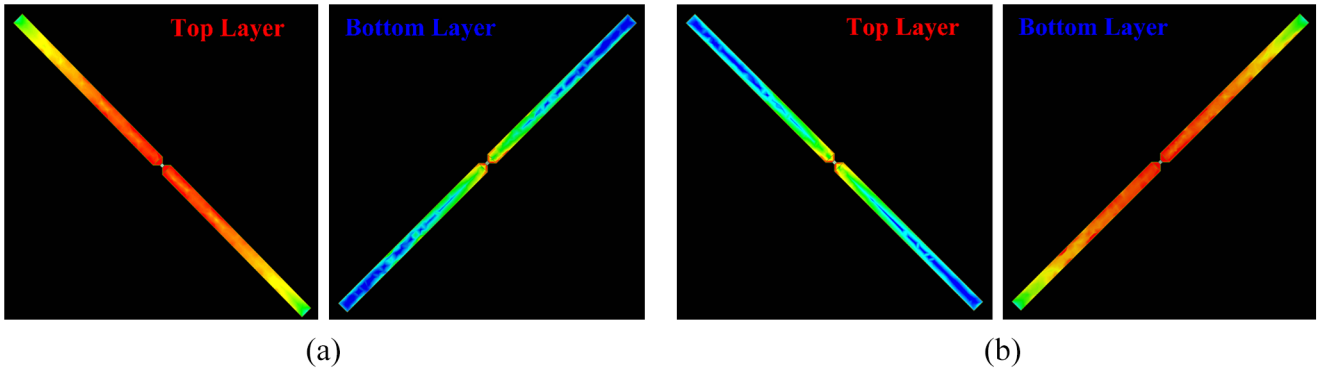


Figure 5. Surface current density distributions of the radiator when the proposed design works in (a) mode 1 and (b) mode 2.

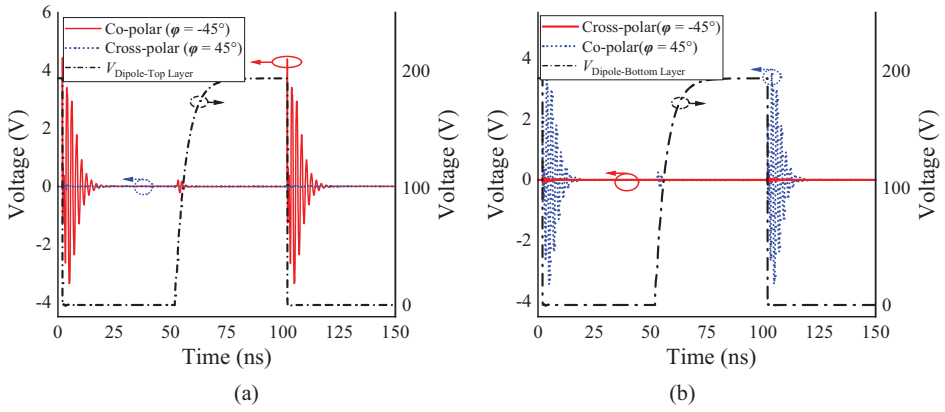


Figure 6. (a) Simulated potential difference $V_{Dipole\text{-}Top\ layer}$ across the dipole radiator on the top layer and the radiated pulses when the pulse transmitter works in mode 1 (co-polar: $\varphi = -45°$; cross-polar: $\varphi = 45°$), as well as (b) the $V_{Dipole\text{-}Bottom\ layer}$ and the radiated pulses in mode 2 (cross-polar: $\varphi = -45°$; co-polar: $\varphi = 45°$).

insertion loss (Typ. 0.25 dB) and high isolation (Typ. 23 dB), is chosen as the SPDT switch. The capacitors C_1, C_2, and C_2' are all 47 pF for the DC block, while the filtering capacitors C_3 and C_3' are both 10 nF. A rectangular wave is introduced as the control signal V_C by the polarization switching network to trigger the target avalanche transistor for oscillation and radiation with the desired polarization. The period, duty cycle, and amplitude of the rectangular wave are 50 μs, 50%, and 1.5 V, respectively.

In the measurement, a standard horn antenna is used as a receiving antenna at a distance of 1.5 m to capture the radiated pulses and transmit the waves to an oscilloscope. The received pulse when the proposed pulse transmitter is working in mode 1 is shown in Fig. 8(a). As observed, the co-polarization of the radiated pulse occurs at a polarization angle of −45° with a peak-to-peak voltage of 1.6 V. By changing the bias voltage V_P, the pulse transmitter transitions to mode 2. As seen from Fig. 8(b), the co-polarization of the radiated pulse changes to the polarization angle of 45°, while the peak-to-peak voltage remains about 1.6 V. Moreover, the power spectrum of the pulses is presented in Fig. 9. As seen, the center frequency of the radiated pulse is about

https://doi.org/10.1017/S175907872510278X Published online by Cambridge University Press

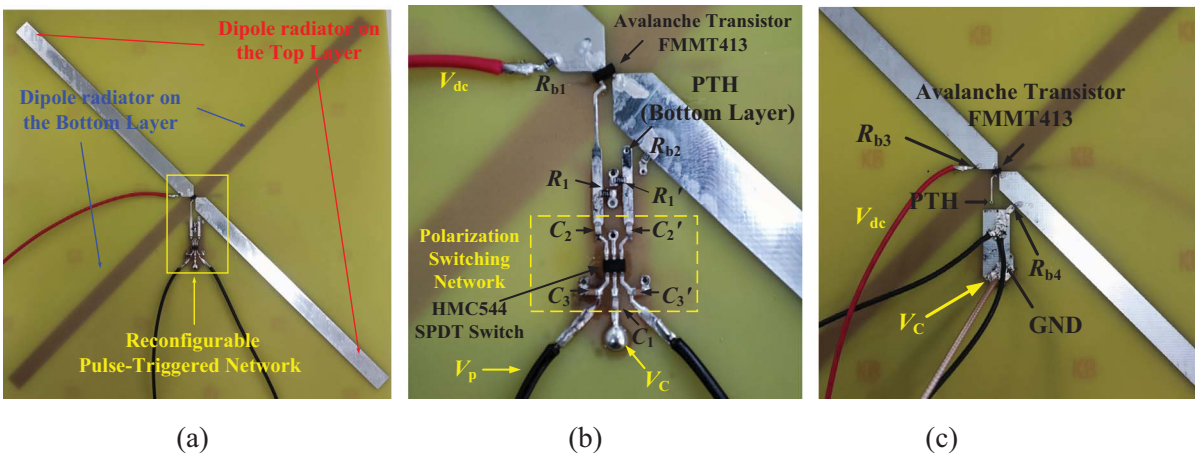


Figure 7. (a) Photograph of the fabricated pulse transmitter, and the (b) top view and (c) bottom view of the reconfigurable pulse-triggered network.

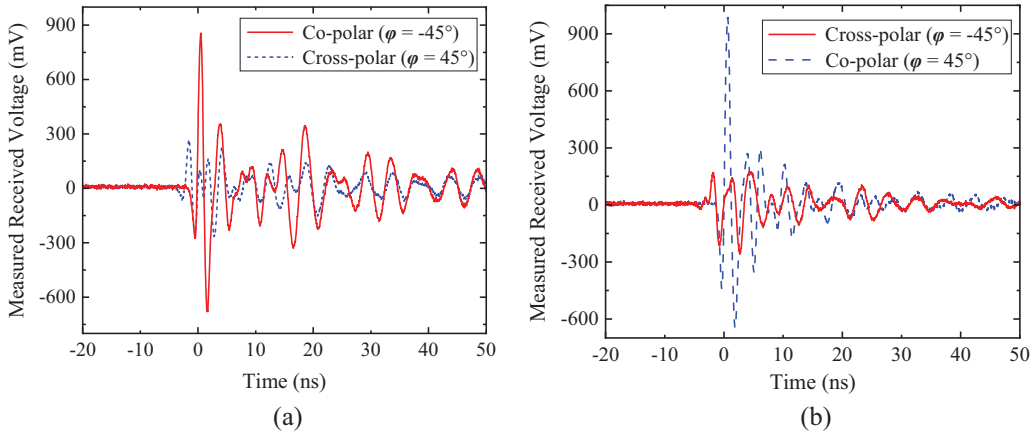


Figure 8. Received pulses from the proposed pulse transmitter working in (a) mode 1 (co-polar: $\varphi = -45°$; cross-polar: $\varphi = 45°$) and (b) mode 2 (cross-polar: $\varphi = -45°$; co-polar: $\varphi = 45°$), respectively.

265 MHz, which depends on the resonant frequency of the passive dipole radiator, as well as the intrinsic capacitance and parasitic elements of the switching transistor, that is, the avalanche transistor FMMT413 used in this test prototype. Note that there are two ways to suppress the undesired frequency components if needed, including adding transmission zeros to the radiator and using cavities or waveguides to house the pulse transmitter. Furthermore, the normalized radiation patterns of the proposed pulse transmitter working in mode 1 and mode 2 are shown in Fig. 10, which agree well with the simulated results.

The comparison among the proposed pulse transmitter based on the self-oscillating AIA and the state-of-the-art self-oscillating AIAs is presented in Table 1. The proposed pulse transmitter based on the self-oscillating AIA can achieve polarization reconfigurability with a competitive high output voltage. Moreover, unlike conventional designs that employ PIN diodes for polarization switching in low-power CW self-oscillating AIA [20], this work presents a method that achieves polarization reconfigurability in high-voltage pulsed self-oscillating AIAs.

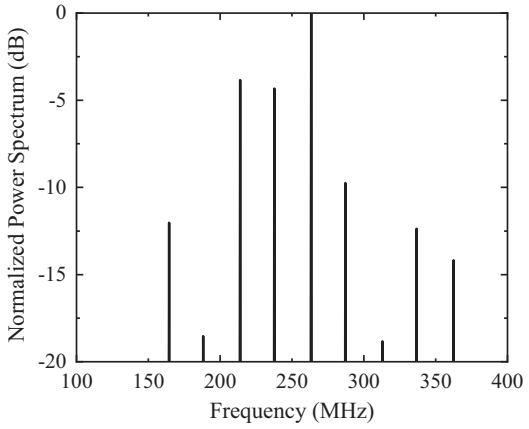


Figure 9. Normalized measured power spectrum of the received pulses from the pulse transmitter.

Conclusion

A polarization-reconfigurable pulse transmitter utilizing a pulse-triggered network has been designed and experimentally validated. This transmitter features a highly integrated structure and operates in two distinct modes corresponding to two orthogonal polarizations. It is capable of directly converting DC energy into radiated pulses with reconfigurable polarization, featuring compact size,

https://doi.org/10.1017/S175907872510278X Published online by Cambridge University Press

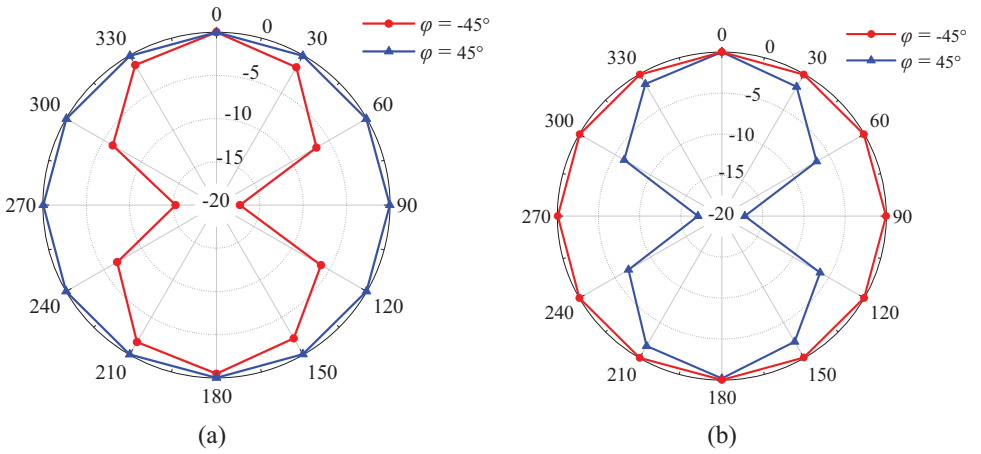


Figure 10. Normalized radiation patterns of the proposed pulse transmitter working in (a) mode 1 and (b) mode 2.

Table 1. Comparison with state-of-the-art self-oscillating AIAs

Ref.	Oscillation frequency (GHz)	Size (λ^2)	Peak-to-peak voltage of the radiated wave[a]	DC–RF efficiency	Polarization reconfigurability
[6]	0.916	0.1	0.01 V @ 3.5 m	19.3%	No
[7]	0.879	0.2	0.021 V @ 1.7 m	26.7%	No
[11]	0.927	0.36	0.05 V @ 3.5 m	29%	No
[12]	0.275 and 0.37	0.03	1.03 V @ 1.5 m	–	No
[14]	0.27	0.023	1.08 V @ 2 m[b]	30%	No
[20]	5.13	1.4	0.006 V @ 2 m	–	Yes
This work	0.265	0.024	1.6 V @ 1.5 m	37%	Yes

[a]Calculated from the received power levels (*Pr*) given in the literature.
[b]AIA unit cell.

low cost, and light weight. It is suitable for applications such as electric effects testing and electro-magnetic interference (EMI).

Acknowledgements. This work was supported by the State Key Laboratory of Millimeter Waves (grant number K202416).

Competing interests. The authors report no conflict of interest.

Author contributions. Manman Cui derived the theory, performed the simulations, and wrote the paper. Jun-Hao Lai performed the simulations and measurements. Huai-Tian Zhou performed the simulations and analyzed data.

References

1. **Wu C-H and Ma T-G** (2014) Miniaturized self-oscillating active integrated antenna with quasi-isotropic radiation. *IEEE Transactions on Antennas and Propagation* **62**, 933–936. https://doi.org/10.1109/TAP.2013.2289942
2. **Huang G-C and Ma T-G** (2024) High-EIRP self-oscillating circularly polarized active integrated crossed-slot antenna. *IEEE Antennas and Wireless Propagation Letters* **23**(1), 54–58, https://doi.org/10.1109/lawp.2023.3317270.
3. **Adhikary M, Biswas A and Akhtar MJ** (2017) Active integrated antenna based permittivity sensing tag. *IEEE Sensors Letters* **1**, 1–4. https://doi.org/10.1109/LSENS.2017.2768560
4. **Lin -Y-Y, Wu C-H and Ma T-G** (2011) Miniaturized self-oscillating annular ring active integrated antennas. *IEEE Transactions on Antennas and Propagation* **59**, 3597–3606. https://doi.org/10.1109/TAP.2011.2163782
5. **Liu Z-H, Chang Y-W and Ma T-G** (2016) High-efficiency self-oscillating active integrated antenna using metamaterial resonators and its application to multicarrier radio frequency identification systems. *IEEE Transactions on Antennas and Propagation* **64**, 3803–3810. https://doi.org/10.1109/TAP.2016.2589959
6. **Tsai Y-L, Chu HN and Ma T-G** (2020) Self-oscillating circularly polarized active integrated monopole antenna using cross-coupled pair and Inverted- L Strip. *IEEE Antennas and Wireless Propagation Letters* **19**, 1132–1136. https://doi.org/10.1109/LAWP.2020.2991467
7. **Ma T-G, Wu X-F, Yeh Y-C and Chu HN** (2022) Self-oscillating circularly polarized active integrated antenna using zeroth-order resonators with boosted conversion efficiency. *IEEE Antennas and Wireless Propagation Letters* **21**, 1353–1357. https://doi.org/10.1109/LAWP.2022.3167741
8. **Ramon ES, Bernal S, Armanious MMH, Tyo JS, Skipper MC and Abdalla MD** (2016) Tunable electrically small conical folded dipole antenna used as a mesoband high-power microwave source. *IEEE Antennas and Wireless Propagation Letters* **15**, 1614–1617.
9. **Tyo JS, Skipper MC, Abdalla MD and Martin JM**. (2017) Compact,backward-radiating helical ntenna for mesoband high-power applications. *IEEE Antennas and Wireless Propagation Letters* **16**, 1699–1702. https://doi.org/10.1109/LAWP.2017.2666813.
10. **Adhikary M, Sahoo SK, Biswas A and Akhtar MJ** (2019) SIW-based self-oscillating concurrent dual-frequency active integrated antenna. *IEEE Antennas and Wireless Propagation Letters* **18**, 1897–1901. https://doi.org/10.1109/LAWP.2019.2932498
11. **Ma T-G, Wu X-F, Yeh Y-C and Chu HN** (2024) High-EIRP self-oscillating circularly polarized active integrated crossed-slot antenna. *IEEE Antennas and Wireless Propagation Letters* **23**, 54–58. https://doi.org/10.1109/LAWP.2023.3317270

12. **Du Z-X, Zhou H-T, Liu J and Guo C** (2024) Compact self-oscillating active integrated loop antenna with concurrent dual-band operation. *IEEE Antennas and Wireless Propagation Letters* **23**, 1070–1074. https://doi.org/10.1109/LAWP.2023.3344287
13. **Du Z-X, Li A, Cui M, Zhang XY and Sievenpiper DF** (2021) A scalable high-power microwave source based on coherent stimulated emission. *IEEE Transactions on Antennas and Propagation* **69**, 7543–7550. https://doi.org/10.1109/TAP.2021.3076126
14. **Du Z-X, Cui M, Zhang Y, Guo C, Zhang G and Zhang XY** (2023) Compact and scalable active-integrated antenna system with both oscillation and amplification characteristics for high-power applications. *IEEE Transactions on Antennas and Propagation* **71**, 7673–7678. https://doi.org/10.1109/TAP.2023.3287685
15. **Wu C-H and Ma T-G** (2013) Self-oscillating Semi-ring active integrated antenna with frequency reconfigurability and voltage-controllability. *IEEE Transactions on Antennas and Propagation* **61**(7), 3880–3885.
16. **Lin -Y-Y and Ma T-G** (2013) Frequency-reconfigurable self-oscillating active antenna with gap-loaded ring radiator. *IEEE Antennas and Wireless Propagation Letters* **12**, 337–340.
17. **Wu C-H and Ma T-G** (2014) Pattern-reconfigurable self-oscillating active integrated antenna with frequency agility. *IEEE Transactions on Antennas and Propagation* **62**, 5992–5999. https://doi.org/10.1109/TAP.2014.2361897
18. **Singh RK, Basu A and Koul SK** (2017) A novel pattern-reconfigurable oscillating active integrated antenna. *IEEE Antennas and Wireless Propagation Letters* **16**, 3220–3223. https://doi.org/10.1109/LAWP.2017.2769798.
19. **Koul SK and Singh RK** (2022) *Reconfigurable Active and Passive Planar Antennas for Wireless Communication Systems*. Cham, Switzerland: Springer Nature.
20. **Singh RK, Basu A and Koul SK** (2016) Asymmetric coupled polarization switchable oscillating active integrated antenna. In *2016 Asia-Pacific Microw*. New Delhi, India: *Conf. (APMC)*, pp. 1–4.



Manman Cui received the B.Eng. Degree from the Xi'an University of Technology, Xi'an, China, in 2011, and the Ph.D. degree from the South China University of Technology, Guangzhou, China, in 2018, respectively. She is currently a lecturer with the Guangzhou University of Chinese Medicine, Guangzhou, China. Her current research interests include wireless power transfer, wireless communication networks, SWIPT systems, and medical IoT.



Jun-Hao Lai received the B.S. degree in electronic science and technology from Guangdong University of Technology, Guangzhou, China, in 2024, where he is currently pursuing an M.S. degree with the School of Integrated Circuits. His research interests include self-oscillating active integrated antenna and retrodirective antenna.



Huai-Tian Zhou received the B.S. degree in electronic information science and technology from Huizhou University, Huizhou, China, in 2022. He received the M.S. degree from the School of Information Engineering, Guangdong University of Technology, Guangzhou, China, in 2025. He currently works as a professional engineer at Samsung Electronics. His research interests include self-oscillating active integrated antenna.

https://doi.org/10.1017/S175907872510278X Published online by Cambridge University Press